Adaptive robust AC optimal power flow considering intrahour uncertainties

Originally published in:
Electric Power Systems Research 216, https://doi.org/10.1016/j.epsr.2022.109082

Funding acknowledgement:
182529 - Power-to-gas and network seasonal storage for promoting the safe penetration of renewables in Switzerland (SNF)

Electric Power Systems Research 216 (2023) 109082

Contents lists available at ScienceDirect

Electric Power Systems Research

journal homepage: www.elsevier.com/locate/epsr

Adaptive robust AC optimal power flow considering intrahour uncertainties

Behnam Akbari, Giovanni Sansavini *

Reliability and Risk Engineering Laboratory, Institute of Energy and Process Engineering, ETH Zurich, Leonhardstrasse 21, 8092 Zurich, Switzerland

ARTICLE INFO

Keywords:
Adaptive robust optimization
Convex relaxation
Optimal power flow
Second-order cone programming
Uncertainty characterization

ABSTRACT

Given the increasing share of variable renewable energy resources (VREs), power system operations need to account for the associated uncertainty with a fine resolution. This paper formulates an adaptive robust optimal power flow, which secures the hourly schedule against uncertain intrahour power injections. The uncertainty is characterized by spatially correlated polytopic sets. Second-order cone programming relaxation is employed to address the nonconvexity of power flow constraints. A sequential convex programming (SCP) procedure is developed to close the relaxation gaps. Due to convexity, the vertices fully represent the uncertainty sets, which alleviates the computational complexity stemming from full recourse. The effectiveness of the proposed solution framework is verified on 14-, 118-, and 588-bus systems with 80% VRE penetration and various uncertainty sizes. The SCP procedure recovers high-quality AC-feasible solutions in 3–17 iterations within 0.1%–41.4% of the planning horizon time span, which makes it suitable for practical use. The robust optimization can prevent load shedding and reduce operational costs by 2.0%–13.6%, while incurring 2.5%–5.0% reduction in VRE utilization.

1. Introduction

The share of renewables in the global and in the European electricity supply is projected to reach 43% and 60% by 2030, respectively, mainly driven by new solar and wind installations [1]. The intrahour volatility of these variable renewable energy resources (VREs) strains the flexible generation and can pose power reserve problems [2]. In addition, their uncertainty challenges the secure and cost-effective operations of power systems relying on conventional deterministic approaches [3,4]. Therefore, probabilistic models with high temporal resolution are required for reliable flexibility assessment and adequate reserve procurement [4,5].

Several optimization methods account for uncertainty in power system operations [6]. *Stochastic optimization* entails generating representative scenarios and minimizing the expected cost. The efficiency and solution quality, however, are sensitive to the scenario selection schemes [7]. Stochastic optimization is applied to various power system problems, e.g., unit commitment [7,8] and optimal power flow (OPF) [9,10]. *Chance-constrained optimization* determines the solution such that the constraints are satisfied with a specified probability. To overcome their computational complexity for AC OPF, the chance constraints are often approximated by tightened deterministic constraints [11–13]. Both stochastic and chance-constrained optimization requires specifying the probability distribution of the uncertainty, which is often unavailable. *Distributionally robust optimization* relaxes this prerequisite and assumes an ambiguity set of probability distributions. Distributionally robust OPF usually relies on linear approximations of power flow equations to achieve tractability [14–16]. In contrast, *robust optimization* assumes no prior knowledge of the uncertainty distribution. Robust optimization has been used to hedge the operations against uncertain power injections from VREs in unit commitment [4,17,18], single-period OPF [19–23], and multiperiod OPF [24,25].

The optimization models should differentiate between the decisions to be made before the uncertainty is revealed (e.g., day-ahead generation scheduling, reserve procurement) and the adaptable decisions after the uncertainty is revealed (e.g., real-time redispatch, reserve activation). Given the continuous nature of power injection uncertainty, this differentiation results in an infinite-dimensional two-stage optimization problem. To alleviate the associated computational complexity, the infinite recourse space is often restricted to affine functions of the uncertain variables [11,12,26], which may sacrifice economic efficiency.

The other computational complexity arises from the nonconvexity of AC power flow equations. Hence, these equations are usually approximated using the DC model [4,8,16,21] and second-order cone (SOCP) and semidefinite (SDP) programming relaxations [12,23,25,26]. The DC model is computationally efficient but neglects power losses and reactive power. The SDP relaxation, on the other hand, offers more

* Corresponding author.
E-mail address: sansavig@ethz.ch (G. Sansavini).

https://doi.org/10.1016/j.epsr.2022.109082
Received 26 September 2022; Received in revised form 18 November 2022; Accepted 13 December 2022
Available online 26 December 2022

accurate solutions but can hardly scale to large networks [25]. The SOCP relaxation offers a compromise between computational efficiency and accuracy. Yet, the SOCP solutions may entail significant optimality gaps [27] and are often infeasible to the original problem, especially when the cost function is not strictly increasing in power injections [28], e.g., due to the zero marginal cost of renewable units. Furthermore, the quality of the SOCP relaxation degrades for large uncertainty sets [25]. In contrast to convex relaxation, convex restriction ensures AC feasibility, but the inner approximation of the feasible region makes the solutions prone to suboptimality, especially if the recourse decisions are restricted to affine policies as in [19,22].

The treatment of the infinite dimensionality resulting from full recourse varies according to the power flow formulation. On the one hand, the full-recourse OPF literature [8,17,18,20,23,25] usually relies on convex approximations of AC power flow equations to capture the infinite recourse space with finite-dimensional models. On the other hand, the full nonconvex AC OPF literature relies on restricting the uncertainty characterization. For instance, the probabilistic AC OPF models in [9,10,24] secure the operation decisions against a finite number of scenarios, providing no robustness guarantees against other possible scenarios. The chance-constrained AC OPF in [11] linearizes the impact of uncertain power injections, which is valid if the uncertainty is small. Therefore, there is a gap in implementing full recourse in response to general continuous uncertainty, while ensuring AC feasibility.

This paper addresses the computational complexity of adaptive robust OPF while ensuring AC feasibility, without resorting to affine policies. A two-stage robust optimization is formulated to solve multihour AC OPF under uncertain intrahour power injections. The first stage is an economic dispatch, and the second stage determines the subhourly redispatch in response to the uncertainty. The optimization secures the schedule against the worst case; yet, it avoids overconservatism by minimizing the base-case costs [4]. The uncertain power injections from VREs and loads are characterized by polytopic uncertainty sets that capture spatial correlations. This allows a skilled yet efficient characterization of high-dimensional uncertainty [29]. Principal component analysis (PCA) is used to enhance the numerical stability of the uncertainty characterization and reduce the computational needs [30]. A column-and-constraint generation (C&CG) [31] procedure is used to enhance the computational tractability. The decomposition greatly benefits from parallel computation and is further expedited by warm starting the set of binding subproblems.

The major contributions are as follows:

1. The proposed adaptive robust OPF employs full recourse for an effective activation of ramping reserves in response to uncertainty realizations. The resulting infinite dimensionality is addressed using SOCP relaxation, which allows to account for the uncertainty sets by enumerating the vertices [32]. The proposed model goes beyond the state-of-the-art SOCP-based robust OPF models with full recourse, namely, (a) in comparison to [25], it retrieves base-case generation setpoints, which the system operator requires in real-world settings, for instance as the dispatch settled in the day-ahead market, and, it extends the uncertainty characterization and the optimization horizon of [23].
2. To recover AC feasibility, a sequential convex programming (SCP) procedure is developed. The SCP procedure is shown to reliably retrieve near-global AC-feasible solutions. In contrast to sequential linear programming [33], the SCP procedure retains convex nonlinear constraints and achieves higher solution stability [34]. Also, this paper improves on previous works employing SOCP relaxation and SCP in the context of robust power system optimizations [35,36], as they are restricted to radial networks. The algorithmic order in [35] guarantees robustness only against the uncertainty boundaries, and [36] ensures AC feasibility only for the worst uncertainty realization. Indeed, the proposed methodology extends robustness guarantees to more general uncertainty characterizations compared to the full AC OPF literature [9–11,24].

The rest of the paper is organized as follows. Section 2 formulates the multiperiod AC OPF model and the extension to an adaptive robust counterpart. Section 3 proposes the solution methods, i.e., a C&CG procedure for tractability and a SCP procedure for AC feasibility. Section 4 presents the results and discusses the computational and practical performance of the solution methods. Section 5 concludes the paper.

2. Mathematical models

2.1. Augmented multiperiod SOCP AC OPF

A nonconvex formulation of the deterministic AC OPF and the SOCP relaxation is introduced; then, the convexified problem is augmented with linearized constraints to tighten the relaxation gaps.

For notation simplicity but with no loss of generality, one generator, one load, and one shunt element are assumed to be located at each bus, and a maximum of one branch connects two buses. The power network can be represented as a simple directed graph with $|\mathcal{B}|$ vertices and $|\mathcal{L}|$ edges.

$\Re(\cdot)$, $\Im(\cdot)$, $(\cdot)^*$, and $\arg(\cdot)$ denote the real value, the imaginary value, the conjugate, and the angle of complex numbers, respectively, and $w_{ijt} = v_{it}v_{jt}^*$ and $\ell_{ijt} = |i_{ijt}|^2$ are defined as lifted voltage and current variables.

The multiperiod AC OPF seeks to minimize generation cost:

$$\min f = \min \sum_{t\in\mathcal{T}} \sum_{i\in\mathcal{B}} C_{2i}\Re\left(s_{it}^g\right)^2 + C_{1i}\Re\left(s_{it}^g\right) + C_{0i}. \tag{1}$$

Voltage magnitude limits (2), generator capability curve (3), available power from generators (4), generator ramping limits (5), and nodal power balance (6) hold $\forall i \in \mathcal{B}, t \in \mathcal{T}$:

$$\underline{V}_i^2 \le w_{iit} \le \overline{V}_i^2 \tag{2}$$

$$A_{ik}\Re\left(s_{it}^g\right) + B_{ik}\Im\left(s_{it}^g\right) \le 1 \quad \forall k \tag{3}$$

$$\Re\left(s_{it}^g\right) \le \overline{p}_{it}^g \tag{4}$$

$$-R_i^d \le \Re\left(s_{it}^g - s_{i(t-1)}^g\right) \le R_i^u \tag{5}$$

$$s_{it}^g - s_{it}^d = Y_i^* w_{iit} + \sum_{(i,j)\in\mathcal{L}} s_{ijt} + \sum_{(j,i)\in\mathcal{L}} s_{ijt}, \tag{6}$$

where A_{ik} and B_{ik} capture the generators' ranges of active power, reactive power, and power factor; $\overline{p}_{it}^g$ models the time-dependent active power available from VREs; s_{it}^g, s_{it}^d, $Y_i^* w_{iit}$, and s_{ijt} are power injections from the generators, loads, shunt elements, and branches, respectively.

Voltage angle difference limits (7), flow limits (8), and power flow equations (9)–(12) hold $\forall (i,j) \in \mathcal{L}, t \in \mathcal{T}$:

$$-\pi/2 < \underline{\theta}_{ij} \le \theta_{ijt} \le \overline{\theta}_{ij} < \pi/2 \tag{7}$$

$$\left|Y_{ij}\right|^2 \left(w_{iit} + w_{jjt} - 2\Re\left(w_{ijt}\right)\right) \le \overline{I}_{ij}^2 \tag{8a}$$

$$\left|s_{ijt}\right|^2 \le \overline{S}_{ij}^2, \left|s_{jit}\right|^2 \le \overline{S}_{ij}^2 \tag{8b}$$

$$s_{ijt} = Y_{ij}^* w_{iit} - Y_{ij}^* w_{ijt} \tag{9a}$$

$$s_{jit} = Y_{ij}^* w_{jjt} - Y_{ij}^* w_{ijt}^* \tag{9b}$$

$$s_{ijt} + s_{jit} = Z_{ij}\ell_{ijt} \tag{10a}$$

$$w_{iit} - w_{jjt} = 2\Re\left(Z_{ij}s_{ijt}^*\right) - \left|Z_{ij}\right|^2 \ell_{ij} \tag{10b}$$

$$\left|w_{ijt}\right|^2 = w_{iit}w_{jjt} \tag{11a}$$

$$\left|s_{ijt}\right|^2 = w_{iit}\ell_{ijt} \tag{11b}$$

$$\theta_{ijt} = \arg\left(w_{ijt}\right) \tag{12a}$$

$$\theta_{ijt} = \arg\left(w_{iit} - Z_{ij}^{*} s_{ijt}\right). \tag{12b}$$

where $\overline{I}_{ij}$ and $\overline{S}_{ijt}$ denote branch current and power limits, respectively, and $Z_{ij} = Y_{ij}^{-1}$ is the branch impedance. The explanation and extensions of (8)–(12) to the full transmission branch model are given in [37].

Constraints (11) and (12) are nonconvex. To mitigate the corresponding complexity, the angle relations (12) are dropped, and the quadratic constraints (11) are relaxed to second-order cones [37]:

$$\left\| \begin{matrix} 2w_{ijt} \\ w_{iit} - w_{jjt} \end{matrix} \right\|_2 \leq w_{iit} + w_{jjt} \tag{13a}$$

$$\left\| \begin{matrix} 2s_{ijt} \\ w_{iit} - \ell_{ijt} \end{matrix} \right\|_2 \leq w_{iit} + \ell_{ijt} \tag{13b}$$

As a result, the extended solution space also includes solutions that are infeasible to the original nonconvex problem. The distance of a solution from feasibility is quantified by *relaxation gaps*:

$$g_{q\,ijt} = w_{iit} w_{jjt} - \left|w_{ijt}\right|^2 \tag{14a}$$

$$g_{q\,ijt} = w_{iit} \ell_{ijt} - \left|s_{ijt}\right|^2 \tag{14b}$$

$$g_{\theta\,ijt} = \left|\theta_{ijt} - \arg\left(w_{ijt}\right)\right| \tag{15a}$$

$$g_{\theta\,ijt} = \left|\theta_{ijt} - \arg\left(w_{iit} - Z_{ij} s_{ijt}\right)\right| \tag{15b}$$

To tighten the relaxation gaps, the relaxed problem is augmented by linearizing (11) and (12) at an initial point $\tilde{x}$:

$$\begin{aligned} &\tilde{w}_{iit} w_{jjt} + \tilde{w}_{jjt} w_{iit} - 2\Re(\tilde{w}_{ijt} w_{ijt}^{*}) \\ &\quad -\tilde{w}_{iit}\tilde{w}_{jjt} + |\tilde{w}_{ijt}|^2 \leq \gamma_{q\,ijt} \end{aligned} \tag{16a}$$

$$\begin{aligned} &\tilde{w}_{iit} \ell_{jjt} + \tilde{\ell}_{jjt} w_{iit} - 2\Re(\tilde{s}_{ijt} s_{ijt}^{*}) \\ &\quad -\tilde{w}_{iit}\tilde{\ell}_{jjt} + |\tilde{s}_{ijt}|^2 \leq \gamma_{q\,ijt} \end{aligned} \tag{16b}$$

$$\left|\theta_{ijt} - \arg\left(\tilde{w}_{ijt}\right) - \frac{\Im\left(\tilde{w}_{ijt}^{*} w_{ijt}\right)}{\left|\tilde{w}_{ijt}\right|^2}\right| \leq \gamma_{\theta\,ijt} \tag{17a}$$

$$\begin{aligned} &\left|\theta_{ijt} - \arg\left(\tilde{w}_{iit} - Z_{ij}^{*}\tilde{s}_{ijt}\right) - \tilde{w}_{iit}\Im\left(Z_{ij} s_{ijt}^{*}\right)\right. \\ &\left. + \left|Z_{ijt}\right|^2 \Im\left(\tilde{s}_{ijt} s_{ijt}^{*}\right) + \Im\left(Z_{ij}\tilde{s}_{ijt}^{*}\right) w_{iit}\right| \leq \gamma_{\theta\,ijt} \end{aligned} \tag{17b}$$

$$\gamma_{q\,ijt} \geq 0 \quad \gamma_{\theta\,ijt} \geq 0, \tag{18}$$

where the slack variables $\gamma_{q\,ijt}$ and $\gamma_{\theta\,ijt}$ approximate the relaxation gaps.

In (11)–(17), (a) and (b) present alternative formulations. Thus, the same symbols are used for alternative relaxation gaps and slack variables for notation simplicity without indicating equality.

Because the slack variables have no upper bound, the feasible region is not restricted by (16) and (17) . A penalty function, comprised of the weighted summation of the slack variables, is included in the objective function:

$$p = \sum_{t\in\mathcal{T}} \sum_{(i,j)\in\mathcal{L}} \left(\tau_{q\,ijt}\gamma_{q\,ijt} + \tau_{\theta\,ijt}\gamma_{\theta\,ijt}\right) \tag{19}$$

The penalty coefficients $\tau_{q\,ijt}$ and $\tau_{\theta\,ijt}$ are parameters set by the SCP procedure, explained in Section 3.2.

The resulting optimization problem is summarized in Table 1 for bus injection (BIM) and branch flow model (BFM) representations.

2.2. Power injection uncertainty sets

Due to their inherent uncertainty, the available power from VREs ($\overline{p}_{it}^{g}$ in (4)) and load power demand (s_{it}^{d} in (6)) deviate from the hourly point forecast. To characterize the intrahour uncertainty, the authors

Table 1
Representations of augmented multiperiod SOCP AC OPF: variables (V), objective function (OF), and constraints (C).

	BIM	BFM	Compact form
V	s_{it}^{g}, w_{iit}, w_{ijt}, θ_{ijt}, $\gamma_{q\,ijt}$, $\gamma_{\theta\,ijt}$	s_{it}^{g}, w_{iit}, s_{ijt}, s_{jit}, ℓ_{ijt}, θ_{ijt}, $\gamma_{q\,ijt}$, $\gamma_{\theta\,ijt}$	$\boldsymbol{x}$
OF	(1) + (19)	(1) + (19)	$f(\boldsymbol{x}) + p(\boldsymbol{x})$
C	(2)–(7), (8a), (9) (13a), (16a), (17a), (18)	(2)–(7), (8b), (10) (13b), (16b), (17b), (18)	$g(\boldsymbol{x}) \leq 0$

denote the uncertain variables at hour t by $\boldsymbol{u}_t \in \mathbb{R}^{d_u}$ and their estimated mean and covariance by $\hat{\boldsymbol{u}}_t$ and $\boldsymbol{\Sigma}_t$, respectively. If some variables are tightly correlated, or if any variable has minute variance, the covariance matrix is ill-conditioned for inversion. Hence, the uncertainty set proposed by Golestaneh et al. [29] is adapted using PCA [38]:

$$\boldsymbol{\Sigma}_t = \boldsymbol{R}_t \boldsymbol{\Lambda}_t \boldsymbol{R}_t^{-1}, \tag{20}$$

where $\boldsymbol{\Lambda}_t$ is a diagonal matrix of eigenvalues (λ_{kt}) and $\boldsymbol{R}_t$ is a matrix whose columns are the right eigenvectors of $\boldsymbol{\Sigma}_t$. Because $\boldsymbol{\Sigma}_t$ is symmetric, $\boldsymbol{R}_t$ is orthonormal, i.e., $\boldsymbol{R}_t^{-1} = \boldsymbol{R}_t^{T}$. The smallest eigenvalue corresponds to the direction along which the variance is minimal. We dismiss eigenvalues that are smaller than a fraction α of the maximum eigenvalue $\max(\lambda_{kt})$ and the associated eigenvectors to obtain $\boldsymbol{\Lambda}'_t \in \mathbb{R}^{d_{ut}\times d_{ut}}$ and $\boldsymbol{R}'_t \in \mathbb{R}^{d_u \times d_{ut}}$.

The principal components of $\boldsymbol{u}_t$ are derived as $\boldsymbol{v}_t = \boldsymbol{R}_t'^{T}\left(\boldsymbol{u}_t - \hat{\boldsymbol{u}}_t\right)$, whose covariance matrix is $\boldsymbol{\Lambda}'_t$. Hence, the uncertainty set is represented as

$$\mathcal{U}_t = \{\boldsymbol{u}_t \in \mathbb{R}^{d_u} : \boldsymbol{u}_t = \boldsymbol{R}'_t \boldsymbol{v}_t + \hat{\boldsymbol{u}}_t, \left\|\boldsymbol{\Lambda}_t'^{-\frac{1}{2}} \boldsymbol{v}_t\right\| \leq \Gamma_t\}, \tag{21}$$

where $\|\cdot\|$ is a 1-norm or ∞-norm for a polytopic set, which is more efficient than other sets, such as ellipsoidal [29]; Γ_t is the scale parameter. If the probability distribution of $\boldsymbol{u}_t$ is known, Γ_t can be selected such that the realizations of $\boldsymbol{u}_t$ lie inside $\mathcal{U}_t$ with a certain probability.

In addition to solving the numerical issues in covariance matrix inversion, the proposed methodology enhances computational efficiency by reducing the uncertainty dimension. Moreover, the proposed uncertainty characterization allows straightforward derivation of the vertices' coordinates; in the case of 1-norm (or ∞-norm), the $2d_{ut}$ (or $2^{d_{ut}}$) vertices are affine images of d_{ut}-dimensional points in the form of $[0, \ldots, \pm\lambda_{k,t}^{\frac{1}{2}}, \ldots, 0]^T$ (or $[\pm\lambda_{1,t}^{\frac{1}{2}}, \ldots, \pm\lambda_{d_{ut},t}^{\frac{1}{2}}]^T$).

2.3. Adaptive robust AC OPF

This section formulates a two-stage robust optimization problem, in which the first-stage decisions, denoted as $\boldsymbol{x}^{b}$, refer to the base-case operation plan, and the second-stage decisions, denoted as $\boldsymbol{x}^{\boldsymbol{u}_t}$, refer to the recourse actions. The first stage optimizes the hourly dispatch schedule, while the second stage determines the subhourly redispatch according to the uncertainty realization. Indeed, the system operator is given full-recourse opportunity to adapt the dispatch schedule in real time in response to the deviation of the uncertain power injections from the point forecast. Unlike affine recourse policy, which distributes the forecast error among conventional generators according to predefined participation factors, the full recourse reoptimizes the dispatch schedule and ensures load balancing by including the nodal power balance (6) also in second-stage constraints. Respecting the electricity markets, the first stage captures energy and reserve procurement, and the second stage represents reserve activation.

The first- and second-stage decisions are linked via

$$-R_i^{-} \leq \Re\left(s_i^{g\,\boldsymbol{u}_t} - s_{it}^{g\,b}\right) \leq R_i^{+} \quad \forall \boldsymbol{u}_t, \tag{22}$$

which imposes the subhourly ramping reserve limits and will be denoted as $h(.)$ henceforth. We also represent the penalty function (19)

and the constraint function (Table 1) of both stages with $p(.)$ and $g(.)$, respectively. The adaptive robust optimization is formulated as

$$\min_{\boldsymbol{x}^b} [f(\boldsymbol{x}^b) + p(\boldsymbol{x}^b) + \max_{\boldsymbol{u}_t} \min_{\boldsymbol{x}^{\boldsymbol{u}_t}} p(\boldsymbol{x}^{\boldsymbol{u}_t})] \tag{23a}$$

$$\text{s.t. } g(\boldsymbol{x}^b) \le 0 \tag{23b}$$

$$h(\boldsymbol{x}^b, \boldsymbol{x}^{\boldsymbol{u}_t}) \le 0 \quad \forall t \tag{23c}$$

$$g(\boldsymbol{x}^{\boldsymbol{u}_t}) \le 0 \quad \forall t \tag{23d}$$

$$\boldsymbol{u}_t \in \mathcal{U}_t \quad \forall t, \tag{23e}$$

which certifies robustness against every realization within the uncertainty sets $\mathcal{U}_t, \forall t$. Yet, (23) in not overconservative because the objective function does not include the worst-case operation costs, namely $\max_{\boldsymbol{u}_t} \min_{\boldsymbol{x}^{\boldsymbol{u}_t}} f(\boldsymbol{x}^{\boldsymbol{u}_t})$.

3. Solution methods

Section 3.1 introduces a decomposition procedure for enhancing computational tractability, Section 3.2 presents a SCP procedure for recovering AC feasibility, Section 3.3 describes the overall solution framework to the adaptive robust OPF, and Section 3.4 discusses the theoretical limitations of the proposed solution framework.

3.1. Column-and-constraint generation

Due to the uncountability of $\mathcal{U}_t$, the problem (23) has infinitely many decision variables $\boldsymbol{x}^{\boldsymbol{u}_t}$ and infinitely many constraints of the form (23c) and (23d). Because $\mathcal{U}_t$ is a polytopic set, and constraints (23c) and (23d) are convex with respect to $\boldsymbol{x}^{\boldsymbol{u}_t}$, the penalty function $p(\boldsymbol{x}^{\boldsymbol{u}_t})$ achieves its maximum at a vertex of $\mathcal{U}_t$ [32]. This property is used to decompose (23) to a master problem (24) and $|\mathcal{V}|$ subproblems (25), where $\mathcal{V}$ is the vertex set of $\mathcal{U}_t$ for all t. Further, if VRE power can be flexibly curtailed, an exact Pareto reduction technique can reduce $\mathcal{V}$ by excluding dominated vertices, corresponding to scenarios with more abundant VRE power.

The master problem includes the first-stage decision variables ($\boldsymbol{x}^b$) and a subset of the second-stage decision variables ($\boldsymbol{x}^v$, $\boldsymbol{v} \in \mathcal{V}^s \subseteq \mathcal{V}$), which pertain to the binding subproblems identified so far:

$$\min\ f(\boldsymbol{x}^b) + p(\boldsymbol{x}^b) + \eta \tag{24a}$$

$$\text{s.t. } g(\boldsymbol{x}^b) \le 0 \tag{24b}$$

$$\eta \ge 0 \tag{24c}$$

$$h(\boldsymbol{x}^b, \boldsymbol{x}^v) \le 0 \quad \forall \boldsymbol{v} \in \mathcal{V}^s \tag{24d}$$

$$\eta \ge p(\boldsymbol{x}^v) \quad \forall \boldsymbol{v} \in \mathcal{V}^s \tag{24e}$$

$$g(\boldsymbol{x}^v) \le 0 \quad \forall \boldsymbol{v} \in \mathcal{V}^s \tag{24f}$$

After solving the master problem, the first-stage decision variables are fixed, and the feasibility of each remaining subproblem $\boldsymbol{v} \in \mathcal{V} \backslash \mathcal{V}^s$ is checked by solving

$$\min\ p(\boldsymbol{x}^v) \tag{25a}$$

$$\text{s.t. } h(\boldsymbol{x}^{b*}, \boldsymbol{x}^v) \le 0 \tag{25b}$$

$$g(\boldsymbol{x}^v) \le 0. \tag{25c}$$

The master problem and the subproblems are incorporated in an iterative C&CG procedure, expressed in Algorithm 1. Each iteration augments the master problem with a binding subproblem, in which the feasible region is empty or the relaxation penalty is larger than those of previous binding subproblems. Although the iterations of Algorithm 1 are sequential, the subproblems within each iteration are independently solvable, enabling high gains from parallel computation.

Ref. [25] also uses C&CG to solve adaptive robust AC OPF, except that the worst-case realization of the uncertainty is determined using an iterative procedure. The proposed methodology, on the other hand, solves the subproblems in parallel and has the flexibility of augmenting the master problem with multiple subproblems at a time. Other primal decompositions (e.g., Benders decomposition and constraint generation) are also applicable when the recourse decision variables are restricted to affine functions of the uncertain variables [39,40]. While primal decompositions rely on fixing complicating variables $\boldsymbol{x}^b$, dual decompositions [41,42] could be used to separate the subproblems by relaxing complicating constraints (24d). The number of complicating constraints is proportional to $|\mathcal{V}|$, which renders dual decompositions unsuitable for large uncertainty dimensions.

Algorithm 1: C&CG Procedure

1. Initialize $\mathcal{V}^s$.
2. Solve the master problem (24) to obtain $\boldsymbol{x}^{b*}$ and η^*.
3. Given the master problem solution, solve subproblems (25) for $\boldsymbol{v} \in \mathcal{V} \backslash \mathcal{V}^s$.
4. If $p(\boldsymbol{x}^v) \le \eta^*$ for all $\boldsymbol{v} \in \mathcal{V} \backslash \mathcal{V}^s$, terminate; otherwise, proceed to step 5.
5. Set $\mathcal{V}^s = \mathcal{V}^s \cup \{\text{argmax}_{\boldsymbol{v} \in \mathcal{V} \backslash \mathcal{V}^s} p(\boldsymbol{x}^v)^\dagger\}$, and go to step 2.

† The objective value of an infeasible subproblem is $+\infty$.

Algorithm 2: SCP Procedure

1. Initialize $\epsilon_{q/\theta^\dagger}$, ϵ_f, $c_{q/\theta}$, $\overline{\tau}_{q/\theta}$, $\underline{\mu}$, $\overline{\mu}$, and $iter = 1$.
2. If $iter = 1$, $\tau^{b/v^\ddagger}_{q/\theta\, ijt} = 0$.
   If $iter = 2$, $\tau^{b/v}_{q/\theta\, ijt} = c_{q/\theta} f\left(\boldsymbol{x}^b_1\right)$.
   If $iter \ge 3$, $\mu^{b/v}_{q/\theta\, ijt} = \min\left(\overline{\mu}, \max\left(\underline{\mu}, g^{b/v}_{q/\theta\, ijt}/\epsilon_{q/\theta}\right)\right)$,
   $\tau^{b/v}_{q/\theta\, ijt} = \min\left(\overline{\tau}_{q/\theta}, \mu^{b/v}_{q/\theta\, ijt}\tau^{b/v}_{q/\theta\, ijt}\right)$.
3. Solve (23) to obtain $\boldsymbol{x}^{b/v}_{iter}$.
4. If $\max\left(g^{b/v}_{q\, ijt}\right) \le \epsilon_q$ and $\max\left(g^{b/v}_{\theta\, ijt}\right) \le \epsilon_\theta$, proceed to step 5; otherwise, jump to step 6.
5. If $iter = 1$ or $\left|f\left(\boldsymbol{x}^b_{iter}\right) - f\left(\boldsymbol{x}^b_{iter-1}\right)\right| \le \epsilon_f . f\left(\boldsymbol{x}^b_{iter-1}\right)$, terminate; otherwise, proceed to step 6.
6. Update the linearization points, i.e., $\tilde{\boldsymbol{x}}^{b/v} = \boldsymbol{x}^{b/v}_{iter}$.
7. Set $iter = iter + 1$ and go to step 2.

† q/θ denotes parameters pertaining to quadratic and angle constraints.
‡ b/v denotes first- and second-stage variables and parameters.

3.2. Sequential convex programming

Although (23) penalizes the linearized relaxation gaps, the relaxation tightness is only preserved with a suitable choice of the linearization point and of penalty coefficients. SCP systematically updates the linearizations and the coefficients until the relaxation gaps are within tolerance and the objective value converges in successive iterations. The authors adapt the SCP procedure proposed in [37] and inspired by [34], which has proven effective in retrieving near-global solutions to power flow optimizations. The procedure is generalized to a two-stage multiperiod optimization and is detailed in Algorithm 2. The first iteration solves (23) with penalty coefficients set to zero. Therefore, the solution gives a lower bound on the objective value of the full AC problem, and if the relaxation gaps are tight, the solution is globally optimal; otherwise, the algorithm augments the objective function with a linearization of the relaxation gaps and resolves (23). The linearization and the solution steps are repeated until the relaxation gaps are within tolerance and the objective value converges in successive iterations.

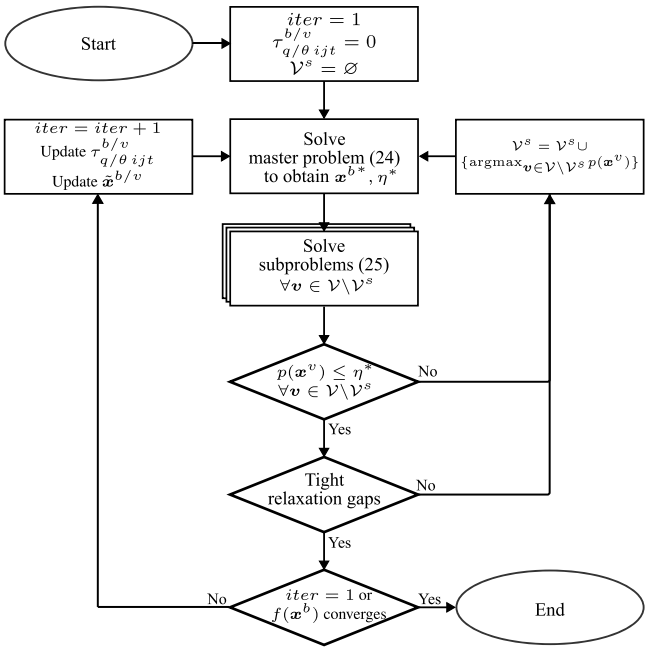

Fig. 1. Flowchart of the overall solution framework.

3.3. Overall solution framework

The C&CG procedure is integrated within the SCP algorithmic loop for solving (23) (Step 3 of Algorithm 2) as depicted in Fig. 1. Therefore, the nonconvexity of the power flow equations is abstracted from the inner loop (Algorithm 1) and treated in the outer loop (Algorithm 2). Such an approach allows the C&CG procedure to guarantee robustness against the entire uncertainty sets by enumerating the finite number of vertices, while the SCP procedures ensures the relaxation gaps are tight in the master problem and the subproblems. Hence, the proposed methodology transcends the state of the art by certifying robustness and AC feasibility simultaneously. Updating the linearization points in Algorithm 2 does not affect the feasible region of individual subproblems. As a result, the set of binding subproblems can only change due to different penalty values over the iterations of Algorithm 2. Hence, the computational efficiency is enhanced by warm starting, namely, the set $\mathcal{V}^s$ in Algorithm 1 is initialized to $\varnothing$ in the first iteration of Algorithm 2; in the next iterations, the set is initialized to the latest $\mathcal{V}^s$.

3.4. Theoretical limitations

1. The convergence of Algorithm 2 to a feasible solution is not theoretically guaranteed. Indeed, the NP-hardness of AC feasibility precludes such a guarantee for any polynomial-time solution algorithm [43,44]. Nevertheless, computational experiments demonstrate consistent convergence of Algorithm 2 to feasible solutions within 3–17 iterations.
2. The proposed solution framework ensures AC feasibility for uncertainty realizations corresponding to the point forecast and the vertices of the uncertainty sets. Yet, AC feasibility is not guaranteed for the interior points of the uncertainty sets. It remains a challenge to theoretically ensure AC feasibility for uncountable uncertainty sets. Computational experiments, however, confirm the AC feasibility of the solutions under > 99.98% of the samples from the interior of the uncertainty sets.

Table 2
Test systems summary.

#Buses	14	118	588
#Branches	20	186	686
#Conventional generators	5	54	95
#Solar farms	3	6	6
#Wind farms	4	6	10
Conventional generators capacity (MW)	399	6515	23 614
Solar farms capacity (MW)	66	1327	3079
Wind farms capacity (MW)	142	2067	8117
Average power demand (MW)	259	4242	13 995

4. Computational results

The test systems are taken from PGLib v20 [45] and modified to host VRE units with a total penetration of 80% as summarized in Table 2. Because the performance of each power flow representation (Table 1) depends on network topology [37], the experiments use the BIM for the strongly meshed 14- and 118-bus systems and the BFM for the weakly meshed 588-bus system. Ramping and ramping reserve limits are set to 0.5 p.u./h for conventional generators.

The models are coded in MATLAB with YALMIP [46]. The experiments are performed on a node with two 64-core AMD EPYC 7742 processors and 512 GB RAM, using MOSEK and IPOPT as SOCP and nonconvex solvers.

VRE generation and load time series are retrieved from [47] in 5-min and 30-min resolutions, respectively. The simulation day is divided into six four-hour intervals; the adaptive robust OPF is run for each interval. The VRE units can operate with a power factor of 0.95 lag to lead [48], and their output power can be curtailed if needed. For VRE uncertainty characterization (21), we use the 1-norm and a scale parameter $\Gamma_t = \Delta\sqrt{d_{vt}}$, where Δ is varied from 0 to 1.5, and the covariance matrix for each forecast hour is estimated using exponential smoothing [49] of the same hour over the 30 days prior to the forecasting date. Load uncertainty can be treated in the same manner but is disregarded given the relatively small intrahour load variability.

4.1. Uncertainty dimension reduction

The PCA is tuned by examining various thresholds $\alpha \max(\lambda_{kt})$ for dismissing eigenvalues. The uncertainty sets $\mathcal{U}_t$ $\forall t$ are constructed with a size of $\Delta = 1$ and threshold ratios $\alpha \in [10^{-4}, 5 \cdot 10^{-1}]$. The optimization (26) computes the distance of each realization $\boldsymbol{u}_t^r$ from the corresponding uncertainty set $\mathcal{U}_t$, and (27) computes the forecast error.

$$d^r = \min_{\boldsymbol{u}_t \in \mathcal{U}_t} \left\| \boldsymbol{u}_t^r - \boldsymbol{u}_t \right\|_2 \tag{26}$$

$$e = \frac{\sum_r d^r}{\sum_r \left\| \boldsymbol{u}_t^r \right\|_1} \tag{27}$$

Fig. 2 shows that the forecast error decreases with reducing the threshold ratio, but there remains a residual forecast error, which indicates that $\mathcal{U}_t$ with the selected uncertainty size does not cover every realization. We select a threshold ratio of $\alpha = 0.01$ at the curves' knees, which results in a forecast error of 0.7%–1.1%.

The Pareto reduction technique is used to further relieve the computational burden. Table 3 reports the number of subproblems for the test systems in each time interval after applying the dimension reduction techniques. More significant reduction is achieved for night hours, when the solar plants have zero output, while the average dimension reduction is 32.4%–40.3% (Table 3, last column).

4.2. Recovering AC-feasible solutions

For assessing the effectiveness of the SCP procedure in recovering AC-feasible solutions, the infeasibility measure is defined as the maximum of the normalized relaxation gaps, i.e., $\max\left\{\max\left(g^{b/v}_{q\,ijt}\right)/\epsilon_q\right.$,

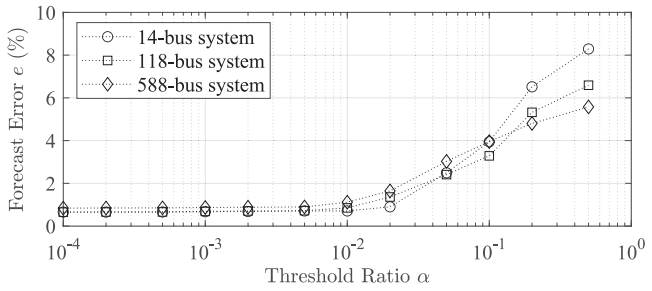

Fig. 2. Evolution of forecast error by varying threshold ratio α in the PCA (uncertainty size $\Delta = 1$).

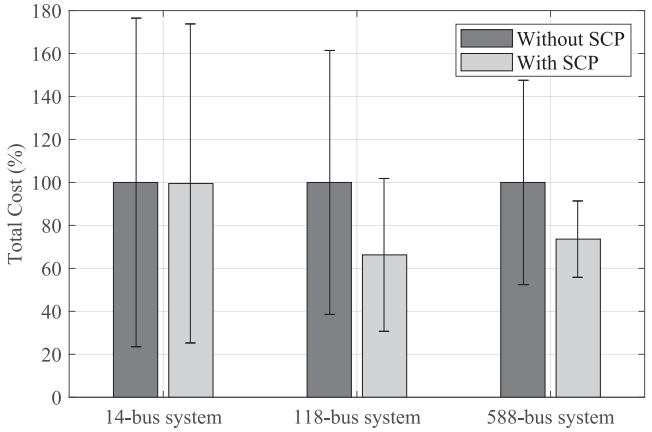

Fig. 3. Total cost of deterministic schedules under realized uncertainty. The error bars show the standard deviations.

Table 3
Number of subproblems after dimension reduction (uncertainty Size $\Delta = 1$).

Test system	Hour range						Dimension
	1–4	5–8	9–12	13–16	17–20	21–24	reduction avg
14-bus system	26	32	42	46	40	31	35.4%
118-bus system	42	51	65	83	65	38	40.3%
588-bus system	72	71	101	121	95	59	32.4%

$\max\left\{g^{b/v}_{\theta ijt}\right)/\epsilon_\theta\}$. If the infeasibility measure is below 1, the relaxation gaps are within tolerance, and the solution is deemed feasible. Table 4 reports the impact of the SCP procedure on the infeasibility measures and the objective values, averaged over the 6 time intervals. The relaxed solutions have high infeasibility values, especially for larger uncertainty sizes. The SCP procedure reduces the infeasibilities by a factor of $1.3 \cdot 10^4$ to $3.6 \cdot 10^6$, yielding solutions appropriate for practical use. Remarkably, the SCP procedure increases the objective values merely $0.1\% - 1.9\%$ on average. The objective value of the global optimum lies between the objective values of the relaxed solution and of the identified feasible solution. The tightness of this interval in the experiments confirms the quality of the solutions retrieved by the SCP procedure. However, the objective values alone should not be used to infer the quality of the relaxed solutions (without the SCP procedure), which may be highly infeasible.

As discussed in Section 3.4, the AC feasibility of the solutions is theoretically guaranteed only for uncertainty realizations corresponding to the point forecast and the vertices of the uncertainty sets. Therefore, experiments are designed to assess the AC feasibility under samples from the interior of the uncertainty sets. A modified exponential spacing [50] is used to draw 1000 samples from the uncertainty set of each hour. A full AC OPF is solved to check the feasibility of adapting the base-case solutions to each uncertainty sample. Table 5 reports the ratio of

Table 4
SCP procedure results: The impact on AC feasibility and objective value.

Uncertainty size (Δ)	0	0.25	0.5	0.75	1	1.25	1.5
14-bus system							
Initial infeasibility ($\times 10^3$)	3.000	3.000	3.000	3.000	3.000	3.000	3.000
Final infeasibility	0.006	0.013	0.012	0.024	0.034	0.037	0.021
Objective value ratio	1.001	1.001	1.001	1.002	1.002	1.001	1.001
118-bus system							
Initial infeasibility ($\times 10^3$)	3.713	3.709	3.769	3.808	3.830	3.846	3.851
Final infeasibility	0.235	0.221	0.205	0.201	0.298	0.249	0.257
Objective value ratio	1.004	1.004	1.005	1.004	1.005	1.005	1.005
588-bus system							
Initial infeasibility ($\times 10^6$)	1.599	1.636	2.646	2.694	2.711	2.713	2.716
Final infeasibility	0.845	0.780	0.735	0.679	0.795	0.800	0.756
Objective value ratio	1.019	1.019	1.018	1.018	1.018	1.018	1.018

Table 5
Ratio of AC-feasible samples from uncertainty sets.

Uncertainty	Without SCP			With SCP		
size (Δ)	0.5	1	1.5	0.5	1	1.5
14-bus system	99.96%	99.92%	99.92%	100.00%	100.00%	100.00%
118-bus system	86.97%	49.98%	86.97%	100.00%	100.00%	100.00%
588-bus system	30.08%	27.42%	32.50%	99.99%	99.99%	99.98%

feasible samples for the three systems under various uncertainty sizes. The SCP procedure achieves a high coverage of the uncertainty sets, while the solutions without SCP show low feasibility ratios for large systems.

4.3. Verification with realized uncertainty

The effectiveness of the proposed framework is verified by assessing robustness against the actual realizations of available VRE power and demand power under a real-world setting of power system operation. The hourly dispatch schedule is retrieved from the robust optimization, and the subhourly redispatch under the realized uncertainty is computed by solving a full nonconvex AC OPF for each 5-minute interval over the course of 24 h. To avoid infeasibility, load shedding is allowed at a cost of 4000 $/MWh [25].

Table 6 shows the key results as average hourly values. Increasing the uncertainty size (Δ) leads to higher generation costs, but lower load shedding costs; the operator can use Δ as a lever to control robustness and achieve the desired compromise between economics and security of supply. The average total cost is minimal at $\Delta = 1$ for the 14-bus system and at $\Delta = 0.75$ for the other two systems. The standard deviation of the total cost is generally decreasing in Δ. Comparing the robust case with minimal cost to the deterministic case ($\Delta = 0$) shows that the robust schedules achieve 2.0%–13.6% cost savings and reductions of cost standard deviation by 43%–81%. Load shedding can be fully avoided by a sufficiently large Δ, but this reduces VRE utilization, because conventional generators replace some renewable generation to ensure enough generation, should VRE output plunge.

The same verification procedure is used for assessing the impact of the SCP procedure under the actual uncertainty realizations. Fig. 3 depicts the total cost associated with deterministic schedules ($\Delta = 0$) with and without SCP for the three test systems. The values are expressed with respect to the average total cost of the cases without SCP. Feasibility recovery using SCP reduces load shedding and thereby cuts the average and the standard deviation of total cost by 0.5%–33.7% and 2.2%–29.8%, respectively.

4.4. Computational performance

Table 7 shows the computational results of solving adaptive robust AC OPF averaged over the instances with uncertainty sizes of $\Delta \in \{0.25,$

Table 6
Practical performance of the proposed robust optimization with different uncertainty sizes under realized uncertainty.

Uncertainty size (Δ)	0	0.25	0.5	0.75	1	1.25	1.5
14-bus system							
Total cost avg ($)	1978	1978	1906	1716	1708	1715	1719
Total cost std ($)	1476	1476	1125	305	281	281	280
Generation cost ($)	1692	1692	1693	1700	1708	1715	1719
Shedding cost ($)	287	287	213	16	0	0	0
Shedding ratio (%)	0.03	0.03	0.02	0.00	0.00	0.00	0.00
VRE utilization (%)	99.59	99.59	99.35	97.52	95.39	93.58	92.47
118-bus system							
Total cost avg ($)	83075	83005	76934	74688	75012	75705	76262
Total cost std ($)	44572	44569	23801	15024	14165	13820	13460
Generation cost ($)	73335	73334	73572	74244	75012	75705	76262
Shedding cost ($)	9740	9671	3362	445	0	0	0
Shedding ratio (%)	0.06	0.06	0.02	0.00	0.00	0.00	0.00
VRE utilization (%)	99.55	99.55	99.39	97.02	93.41	89.98	86.96
588-bus system							
Total cost avg ($)	340206	339058	335900	333386	335193	336914	338383
Total cost std ($)	82116	82151	59395	46915	46575	46605	46871
Generation cost ($)	326502	326741	329649	332112	333857	335396	336491
Shedding cost ($)	13704	12316	6250	1274	1336	1518	1892
Shedding ratio (%)	0.03	0.02	0.01	0.00	0.00	0.00	0.00
VRE utilization (%)	98.25	98.09	96.32	93.21	90.58	88.23	86.76

Table 7
Computational performance of Algorithm 2 in solving 4-hour adaptive robust AC OPF.

Test system	Computation time (s)				#Iter. avg
	Total avg	Total std	Iter. 1 avg	Iter. >1 avg per iter.	
14-bus system	6.8	1.6	4.0	1.4	3.0
118-bus system	72.6	25.9	38.3	10.1	4.4
588-bus system	3774.4	853.8	962.3	310.0	10.4

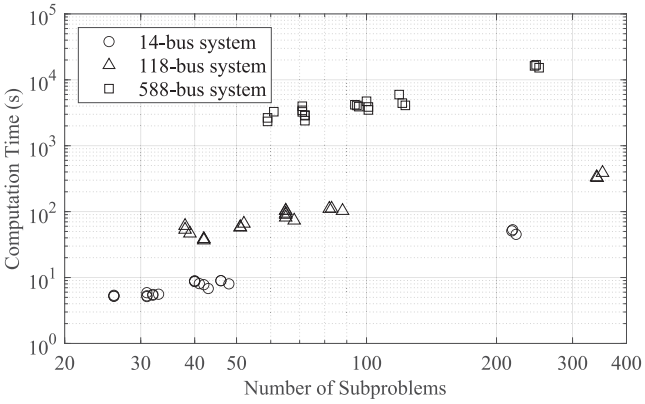

Fig. 4. Computation time of Algorithm 2 for solving adaptive robust OPF.

0.5, 0.75, 1.0, 1.25, 1.5} and the 6 time intervals. The maximum total computation times for the 14-, 118-, and 588-bus systems are 10.7 s, 114.3 s, and 5964.1 s, respectively, well shorter than the planning horizon of 4 h. Comparing the time spent in the initial and in the next iterations of Algorithm 2 reveals that the proposed warm-starting technique almost triples the convergence speed of the C&CG procedure. As a result, a significant fraction of the computation time is spent in the first iteration of the SCP procedure, which amounts to a conventional convex robust optimization without AC feasibility recovery. The SCP procedure converges in 3–16 iterations in all of the 108 instances.

To assess scalability, the solution framework is also used to solve adaptive robust optimization with a planning horizon of 24 h. While a threshold ratio of $\alpha = 0.01$ is used for the smaller test systems, $\alpha = 0.10$ is used for the 588-bus system to restrict the RAM usage to the allocated 512 GB. The average computation times for the 14-, 118-, and 588-bus systems are 1, 6, and 267 min, respectively, and the number of SCP iterations is 3–17. Fig. 4 collects the computational results of 4-hour and 24-hour planning horizons. The computation time almost linearly increases with the number of subproblems.

5. Conclusion

This paper proposes a reliable solution framework for robust multi-period optimal power flow under intrahour power injection uncertainties. SOCP relaxation is used to address the computational complexity arising from the full recourse and the nonconvexity of power flow constraints. To close the relaxation gaps, a sequential convex programming (SCP) procedure is developed, while a column-and-constraint generation (C&CG) procedure is used to enhance the computational tractability.

The experiments on test systems of various sizes show that the proposed framework recovers high-quality AC-feasible solutions for all uncertainty sizes within 3–17 iterations of the SCP procedure. Thanks to the convex relaxation and the proposed technique to warm start the C&CG procedure, the solution framework remains computationally fast for systems of moderate size.

The results indicate that the robust optimization can reduce the operation costs by 2.0%–13.6%, while enhancing the security of supply. Curtailing renewable power becomes inevitable in power systems with high VRE penetration to ensure robustness against sharp declines in VRE power. This finding motivates investigating the installation of new fast-ramping units and storages to increase renewable utilization.

Transmission and generation asset contingencies are among the other short-term uncertainties that power systems face. Thus, an extension of the proposed framework entails integrating security constraints similarly to the subproblems related to uncertain power injections.

CRediT authorship contribution statement

Behnam Akbari: Conceptualization, Methodology, Software, Formal analysis, Investigation, Data curation, Writing – original draft, Visualization. **Giovanni Sansavini:** Conceptualization, Methodology, Resources, Writing – review & editing, Supervision, Funding acquisition.

Declaration of competing interest

The authors declare that they have no known competing financial interests or personal relationships that could have appeared to influence the work reported in this paper.

Data availability

Data will be made available on request.

Acknowledgments

This work is supported by the Swiss National Science Foundation - Project funding in Mathematics, Natural and Engineering Sciences (Division II) - Project number 200021_182529 and the Swiss Federal Office of Energy's SWEET programme as part of the PATHFNDR project. The authors gratefully acknowledge the five anonymous reviewers for their helpful comments and suggestions.

References

[1] International Energy Agency, World Energy Outlook 2022, World Energy Outlook, OECD, 2022, http://dx.doi.org/10.1787/3a469970-en.
[2] EWEA, Wind Energy - the Facts: A Guide To the Technology, Economics and Future of Wind Power, Earthscan, London, 2009.
[3] N. Navid, G. Rosenwald, Market solutions for managing ramp flexibility with high penetration of renewable resource, IEEE Trans. Sustain. Energy 3 (4) (2012) 784–790, http://dx.doi.org/10.1109/TSTE.2012.2203615.
[4] M.I. Alizadeh, M.P. Moghaddam, N. Amjady, Multistage multiresolution robust unit commitment with nondeterministic flexible ramp considering load and wind variabilities, IEEE Trans. Sustain. Energy 9 (2) (2018) 872–883, http://dx.doi.org/10.1109/TSTE.2017.2764061.
[5] J. Deane, G. Drayton, B.Ó. Gallachóir, The impact of sub-hourly modelling in power systems with significant levels of renewable generation, Appl. Energy 113 (2014) 152–158, http://dx.doi.org/10.1016/j.apenergy.2013.07.027.
[6] L.A. Roald, et al., Power systems optimization under uncertainty: A review of methods and applications, Electr. Power Syst. Res. 214 (2023) 108725, http://dx.doi.org/10.1016/j.epsr.2022.108725.
[7] Y. Dvorkin, Y. Wang, H. Pandzic, D. Kirschen, Comparison of scenario reduction techniques for the stochastic unit commitment, in: 2014 IEEE PES Gen. Meet, 2014, pp. 1–5, http://dx.doi.org/10.1109/PESGM.2014.6939042.
[8] A. Antenucci, G. Sansavini, Gas-constrained secure reserve allocation with large renewable penetration, IEEE Trans. Sustain. Energy 9 (2) (2018) 685–694, http://dx.doi.org/10.1109/TSTE.2017.2756091.
[9] A. Nasri, A.J. Conejo, S.J. Kazempour, M. Ghandhari, Minimizing wind power spillage using an OPF with FACTS devices, IEEE Trans. Power Syst. 29 (5) (2014) 2150–2159, http://dx.doi.org/10.1109/TPWRS.2014.2299533.
[10] M. Isuru, E.Y.S. Foo, H.B. Gooi, A piecewise-affine decision rule based stochastic AC optimal power flow approach, in: 2020 IEEE Power Energy Soc. Gen. Meet. PESGM, 2020, pp. 1–5, http://dx.doi.org/10.1109/PESGM41954.2020.9281413.
[11] L. Roald, G. Andersson, Chance-constrained AC optimal power flow: Reformulations and efficient algorithms, IEEE Trans. Power Syst. 33 (3) (2018) 2906–2918, http://dx.doi.org/10.1109/TPWRS.2017.2745410.
[12] A. Venzke, L. Halilbasic, U. Markovic, G. Hug, S. Chatzivasileiadis, Convex relaxations of chance constrained AC optimal power flow, IEEE Trans. Power Syst. 33 (3) (2018) 2829–2841, http://dx.doi.org/10.1109/TPWRS.2017.2760699.
[13] Y. Yi, G. Verbič, Fair operating envelopes under uncertainty using chance constrained optimal power flow, Electr. Power Syst. Res. 213 (2022) 108465, http://dx.doi.org/10.1016/j.epsr.2022.108465.
[14] Y. Guo, K. Baker, E. Dall'Anese, Z. Hu, T.H. Summers, Data-based distributionally robust stochastic optimal power Flow—Part I: Methodologies, IEEE Trans. Power Syst. 34 (2) (2019) 1483–1492, http://dx.doi.org/10.1109/TPWRS.2018.2878385.
[15] L. Yao, X. Wang, Y. Li, C. Duan, X. Wu, Distributionally robust chance-constrained AC-OPF for integrating wind energy through multi-terminal VSC-HVDC, IEEE Trans. Sustain. Energy 11 (3) (2020) 1414–1426, http://dx.doi.org/10.1109/TSTE.2019.2927135.
[16] R.A. Jabr, Distributionally robust CVaR constraints for power flow optimization, IEEE Trans. Power Syst. 35 (5) (2020) 3764–3773, http://dx.doi.org/10.1109/TPWRS.2020.2971684.
[17] N. Amjady, S. Dehghan, A. Attarha, A.J. Conejo, Adaptive robust network-constrained AC unit commitment, IEEE Trans. Power Syst. 32 (1) (2017) 672–683, http://dx.doi.org/10.1109/TPWRS.2016.2562141.
[18] H. Ye, Z. Li, Robust security-constrained unit commitment and dispatch with recourse cost requirement, IEEE Trans. Power Syst. 31 (5) (2016) 3527–3536, http://dx.doi.org/10.1109/TPWRS.2015.2493162.
[19] D. Lee, K. Turitsyn, D.K. Molzahn, L. Roald, Robust AC optimal power flow with robust convex restriction, IEEE Trans. Power Syst. (2021) 1, http://dx.doi.org/10.1109/TPWRS.2021.3075925.
[20] A. Attarha, N. Amjady, A.J. Conejo, Adaptive robust AC optimal power flow considering load and wind power uncertainties, Int. J. Electr. Power Energy Syst. 96 (2018) 132–142, http://dx.doi.org/10.1016/j.ijepes.2017.09.037.
[21] L. Zeng, H.-D. Chiang, D. Liang, Robust optimal power flow under renewable uncertainty with pairwise convex hull and non-affine AGC redispatch strategy, Electr. Power Syst. Res. 210 (2022) 108136, http://dx.doi.org/10.1016/j.epsr.2022.108136.
[22] R. Louca, E. Bitar, Robust AC optimal power flow, IEEE Trans. Power Syst. 34 (3) (2019) 1669–1681, http://dx.doi.org/10.1109/TPWRS.2018.2849581.
[23] H. Yang, D.P. Morton, C. Bandi, K. Dvijotham, Robust optimization for electricity generation, Inf. J. Comput. (2020) http://dx.doi.org/10.1287/ijoc.2020.0956.
[24] T. Soares, R.J. Bessa, P. Pinson, H. Morais, Active distribution grid management based on robust AC optimal power flow, IEEE Trans. Smart Grid 9 (6) (2018) 6229–6241, http://dx.doi.org/10.1109/TSG.2017.2707065.
[25] Á. Lorca, X.A. Sun, The adaptive robust multi-period alternating current optimal power flow problem, IEEE Trans. Power Syst. 33 (2) (2018) 1993–2003, http://dx.doi.org/10.1109/TPWRS.2017.2743348.
[26] M. Chamanbaz, F. Dabbene, C.M. Lagoa, Probabilistically robust AC optimal power flow, IEEE Trans. Control Netw. Syst. 6 (3) (2019) 1135–1147, http://dx.doi.org/10.1109/TCNS.2019.2921300.
[27] C. Coffrin, H.L. Hijazi, P. Van Hentenryck, The QC relaxation: A theoretical and computational study on optimal power flow, IEEE Trans. Power Syst. 31 (4) (2016) 3008–3018, http://dx.doi.org/10.1109/TPWRS.2015.2463111.
[28] S.H. Low, Convex relaxation of optimal power Flow—Part II: Exactness, IEEE Trans. Control Netw. Syst. 1 (2) (2014) 177–189, http://dx.doi.org/10.1109/TCNS.2014.2323634.
[29] F. Golestaneh, P. Pinson, H.B. Gooi, Polyhedral predictive regions for power system applications, IEEE Trans. Power Syst. 34 (1) (2019) 693–704, http://dx.doi.org/10.1109/TPWRS.2018.2861705.
[30] J. Cheng, R. Li-Yang Chen, H.N. Najm, A. Pinar, C. Safta, J.-P. Watson, Distributionally robust optimization with principal component analysis, SIAM J. Optim. 28 (2) (2018) 1817–1841, http://dx.doi.org/10.1137/16M1075910.
[31] B. Zeng, L. Zhao, Solving two-stage robust optimization problems using a column-and-constraint generation method, Oper. Res. Lett. 41 (5) (2013) 457–461, http://dx.doi.org/10.1016/j.orl.2013.05.003.
[32] K. Margellos, P. Goulart, J. Lygeros, On the road between robust optimization and the scenario approach for chance constrained optimization problems, IEEE Trans. Automat. Control 59 (8) (2014) 2258–2263, http://dx.doi.org/10.1109/TAC.2014.2303232.
[33] A. Castillo, P. Lipka, J.-P. Watson, S.S. Oren, R.P. O'Neill, A successive linear programming approach to solving the IV-ACOPF, IEEE Trans. Power Syst. 31 (4) (2016) 2752–2763, http://dx.doi.org/10.1109/TPWRS.2015.2487042.
[34] R.R. Jha, A. Dubey, Network-level optimization for unbalanced power distribution system: Approximation and relaxation, IEEE Trans. Power Syst. 36 (5) (2021) 4126–4139, http://dx.doi.org/10.1109/TPWRS.2021.3066146.
[35] Ahmed R. Sayed, C. Wang, J. Zhao, T. Bi, Distribution-level robust energy management of power systems considering bidirectional interactions with gas systems, IEEE Trans. Smart Grid 11 (3) (2020) 2092–2105, http://dx.doi.org/10.1109/tsg.2019.2947219.
[36] J. Zhang, M. Cui, Y. He, Multi-period fast robust optimization for partial distributed generators (DGs) providing ancillary services, Energies 14 (16) (2021) 4911, http://dx.doi.org/10.3390/en14164911.
[37] B. Akbari, G. Sansavini, Sequential second-order cone programming for AC load maximization problems, in: 2022 IEEE Int. Energy Conf. ENERGYCON, 2022, http://dx.doi.org/10.1109/ENERGYCON53164.2022.9830451.
[38] S. Wold, K. Esbensen, P. Geladi, Principal component analysis, Chemometr. Intell. Lab. Syst. 2 (1-3) (1987) 37–52, http://dx.doi.org/10.1016/0169-7439(87)80084-9.
[39] Á. Lorca, X.A. Sun, E. Litvinov, T. Zheng, Multistage adaptive robust optimization for the unit commitment problem, Oper. Res. 64 (1) (2016) 32–51, http://dx.doi.org/10.1287/opre.2015.1456.
[40] A. Venzke, S. Chatzivasileiadis, Convex relaxations of probabilistic AC optimal power flow for interconnected AC and HVDC grids, IEEE Trans. Power Syst. 34 (4) (2019) 2706–2718, http://dx.doi.org/10.1109/TPWRS.2019.2895122.
[41] S. Mhanna, G. Verbič, A.C. Chapman, Adaptive ADMM for distributed AC optimal power flow, IEEE Trans. Power Syst. 34 (3) (2019) 2025–2035, http://dx.doi.org/10.1109/TPWRS.2018.2886344.
[42] J. Iria, P. Scott, A. Attarha, D. Gordon, E. Franklin, MV-LV network-secure bidding optimisation of an aggregator of prosumers in real-time energy and reserve markets, Energy 242 (2022) 122962, http://dx.doi.org/10.1016/j.energy.2021.122962.
[43] K. Lehmann, A. Grastien, P. Van Hentenryck, AC-feasibility on tree networks is NP-hard, IEEE Trans. Power Syst. 31 (1) (2016) 798–801, http://dx.doi.org/10.1109/TPWRS.2015.2407363.
[44] D. Bienstock, A. Verma, Strong NP-hardness of AC power flows feasibility, Oper. Res. Lett. 47 (6) (2019) 494–501, http://dx.doi.org/10.1016/j.orl.2019.08.009.

[45] S. Babaeinejadsarookolaee, et al., The power grid library for benchmarking AC optimal power flow algorithms, 2019.
[46] J. Lofberg, YALMIP: A toolbox for modeling and optimization in MATLAB, in: 2004 IEEE Int. Conf. Robot. Autom, 2004, pp. 284–289, http://dx.doi.org/10.1109/CACSD.2004.1393890.
[47] Generation and Load, https://aemo.com.au/energy-systems/electricity/national-electricity-market-nem/data-nem/market-management-system-mms-data/generation-and-load.
[48] J. McDowell, et al., Reactive Power Interconnection Requirements for PV and Wind Plants: Recommendations To NERC, Tech. Rep. SAND2012-1098, 2012, 1039006, http://dx.doi.org/10.2172/1039006.
[49] V. Zakamulin, A test of covariance-matrix forecasting methods, JPM 41 (3) (2015) 97–108, http://dx.doi.org/10.3905/jpm.2015.41.3.097.
[50] L. Devroye, Non-Uniform Random Variate Generation, Springer, New York Heidelberg, 1986.